Advances in Nano Research, *Vol. 8, No. 3 (2020) 255-264*
DOI: https://doi.org/10.12989/anr.2020.8.3.255

Post-buckling analysis of aorta artery under axial compression loads

Şeref Doğuşcan Akbaş [1a], Kadir Mercan [2b] and Ömer Civalek*[3]

[1] *Bursa Technical University, Department of Civil Engineering, Yıldırım Campus, 16330, Yıldırım/Bursa, Turkey*
[2] *Mehmet Akif Ersoy University, Faculty of Engineering-Architecture,*
Civil Engineering Department, Division of Mechanics, 15030, Burdur, Turkey
[3] *China Medical University, Taichung, Taiwan*

(*Received October 19, 2019, Revised January 23, 2020, Accepted April 19, 2020*)

Abstract. Buckling and post-buckling cases are often occurred in aorta artery because it affected by higher pressure. Also, its stability has a vital importance to humans and animals. The loss of stability in arteries may lead to arterial tortuosity and kinking. In this paper, post-buckling analysis of aorta artery is investigated under axial compression loads on the basis of Euler-Bernoulli beam theory by using finite element method. It is known that post-buckling problems are geometrically nonlinear problems. In the geometrically nonlinear model, the Von Karman nonlinear kinematic relationship is employed. Two types of support conditions for the aorta artery are considered. The considered non-linear problem is solved by using incremental displacement-based finite element method in conjunction with Newton-Raphson iteration method. The aorta artery is modeled as a cylindrical tube with different average diameters. In the numerical results, the effects of the geometry parameters of aorta artery on the post-buckling case are investigated in detail. Nonlinear deflections and critical buckling loads are obtained and discussed on the post-buckling case.

Keywords: aorta artery; post-buckling analysis; finite element method; Von Karman nonlinear

1. Introduction

Aorta artery attracts most importance since it's vitality among all arteries for humans and mammals (Kaniowsk *et al*. 1970). Also, aorta is the artery with largest diameter and comes out from left ventricle of hearth then sprawl toward lower abdomen to arterials (Jainandunsing *et al*. 2019). The main role of this artery is to transmit oxygenated blood firstly to arterials then to capillary networks. As aorta is the first artery coming out from hearth, highest pressures occur in aorta artery compared to any other artery or capillary (Levy and Tedgui 2007). In humans, the average load of aorta is from 3 to 7 liters per minute (approximately 100 ml per second) depending on age, weight and height. Furthermore, it is known that the pressure in aorta is 80-140 mmHg up to the strength of hearth and physical properties of body (Jezkova *et al*. 2016). Decreasing in thickness of arteries is normally expected to increase the pressure in the blood, while the situation in the arteries is more complicated. The inner-pressure of arteries is not decreasing linearly depending on diameter and length. Inner-pressure is directly depending on the distance of artery from the hearth. As the distance is increasing, in capillaries with diameter between 50 μm-250 μm (approximately 5000 times narrower than aorta) the inner-pressure decreases by 30-40% compared with aortic artery (Gore 1974, Levesque and Nerem 1985, Mulvany and Aalkjaer 1990). The largest pressure drop is between the interstitial terminal arteries, on the other hand blood vessels with diameters less than about 60 μm have no correlation between central blood pressure and microvascular pressure, indicating that pressure is controlled in such small diameter vessels which means the pressure in aorta is far from being controlled (Gore and Bohlen 1975). Blood pressure creates intraluminal pressure from the inner surface of the vessel, resulting in pressure and shear stresses in the vessel wall (Liu *et al*. 2014). In comparison, due to the blood flow, the shear stresses caused by the friction force between the blood and the inner wall of the vessel are transferred to the vessel surface in the same way and can reach critical values to cause buckling in artery. It is also known that the buckling and post-buckling behaviours of the stent by cross sectional analysis after deployment is more important during some operation or biomedical area.

Owing to the development of technology and medical sciences, the attenuation of aortic arteries due to alcohol, aging, obesity, or smoking has become more curable while the incidence of fatal Traumatic Aortic Rupture (TAR) cases as a result of traffic accidents has increased with the increase in the number of vehicles in traffic and the increasing number of accidents. Serious researches has recently begun on the sprains of the aortic artery and its associated tearing. According to these studies, TAR is seen in a small percentage of traffic accidents (1.2%), but it is seen in a significant proportion of fatal traffic accidents (20%). This rate is dramatically high for passengers than drivers in traffic accidents. Traumatic Aortic Rupture (TAR) was observed in 91-99% of passengers who died in fatal traffic accidents (depending on the direction of the force

*Corresponding author, Professor,
E-mail: civalek@yahoo.com
[a] Ph.D., E-mail: serefda@yahoo.com
[b] Ph.D. Student, E-mail: kmercan@mehmetakif.edu.tr

 ISSN: 2287-237X (Print), 2287-2388 (Online)

acting on the vehicle in the traffic accident). Even in cases without TAR, it is observed that, after a non-fatal traffic accident the patient could die within the first 24 hours of arriving at a health center due to Traumatic Aortic Injury (TAI) (Lee *et al*. 2011). According to a study published by Richen *et al*. (2003) 7076 traffic accidents were examined in the UK between 1992 and 1999, resulting in the fact that the wearing of a seat belt or an air bag did not eliminate the possibility of injury in the aortic artery. This situation has revealed the need to study the mechanical causes under TAR and TAI cases for better understanding of critical situations. Determining the critical limits of TAR and TAI cases will lead to development of driver and passenger safety in car safety design. TAR and TAI cases, which are seen in high rate in traffic accidents, occur with more than one deformation (Gammie *et al*. 1998). Almost all traumatic ruptures seen in the aortic artery usually occur in the vertical direction in the form of a cross tear starting from intima (Bertrand *et al*. 1998). Although TAI and TAR were the major part of the fatal cases in traffic accidents, it was found that the single factor parameter does not cause TAR or TAI and the combination of different factors create tension and pressure in the aortic artery exceeding the damage and tear levels. The most effective way of understanding TAR and TAI is to examine and understand the mechanical behavior of the aortic artery under various loads that cause injury or damage.

Some studies in the literature have shown that blood pressure in the aortic artery does not only create an increase in stresses on the vascular surface, but also can affect the straight form of aorta to buckled form (Smyth and Edwards 1972, Han 2009a, b, Rachev 2009). Due to the buckling, a great increase in the tension and pressure in the aortic artery can occur and this increase may lead to cases of TAR and TAI and other types of fatal cases (Agah 2015).

In 2007, Han have published an article which is important to understand the biomechanical properties and behavior of artery buckling (Han 2007). Artery is modeled as linear-elastic, thin-walled in shape of circular cylinders. Constant internal pressure and axial tension with axial elongation have been applied to model. Semi-inverse approach has been applied to obtain buckling equation. As experimental observations indicated that buckling occurs in sin shape, Euler column buckling has been used. The effect of dimensional parameters with axial stretch ratio on stability of arteries have been clearly demonstrated in results.

More recently, experimental studies on mouse and pork aortic arteries have shown that blood pressure and axial stress are the major factors in aortic artery buckling (Hayman *et al*. 2013, Zhang *et al*. 2014). In addition, these studies have shown that vessel buckling form asymmetric regional stresses on the vessel wall and this situation affects the normal behavior and strength of the vessel. Some studies demonstrated that the aortic artery was unstable due to increased blood pressure or reduced axial stress (Han 2009b, Han *et al*. 2013). Martinez *et al*. (2010) have investigated the buckling pressure and to measure the mechanical properties of veins using porcine jugular veins. Later, Liu and Han (2012) investigated the critical buckling pressure of artery under pulsatile pressure using experiments and theoretic works. Following, the torsional buckling of arteries and veins were investigated by Garcia *et al*. (2013, 2017) experimentally using porcine common carotid arteries. These researches and formers contributed much on account of understanding the mechanical properties and behavior of arteries and veins (Han *et al*. 2013).

The experimental study of the human artery under mechanical stress is a very difficult task both ethically and economically. Therefore, it would be more appropriate to examine the aortic artery by mechanically modeling under various loads and examine its buckling and post-buckling behavior.

Buckling analysis have been widely researched and applied to small scaled structures like arteries while it is also applied to nano scaled structures like nanomaterials using higher order theories such as nonlocal elasticity theory, couple-stress theory, strain gradient theory (Demir and Civalek 2007a, Civalek and Demir 2011a, b, Akgöz and Civalek 2013, Youcef *et al*. 2015, Tornabene *et al*. 2015b, Kheroubi *et al*. 2016, Akgöz and Civalek 2016, 2017a, b, Mercan and Civalek 2017, Semmah *et al*. 2019, Ebrahimi *et al*. 2019). Also, vibration analysis of small and nano sized structures has been researched during last decades (Civalek and Kiracioglu 2010, Akgöz and Civalek 2014, 2017c, Demir and Civalek 2013, 2017b, Demir *et al*. 2017, Ebrahimi and Barati 2017, 2018, Fantuzzi *et al*. 2017, Berghouti *et al*. 2019, Bendaho *et al*. 2019). Furthermore, dynamic analysis has been also applied to small and nano sized structrures (Tornabene *et al*. 2015a, Civalek and Demir 2016, Numanoglu *et al*. 2018, Jalaei and Arani 2018, Jalaei *et al*. 2018, Butaleb *et al*. 2019). On the other side, molecular dynamic analysis method has been gained popularity due to overcoming modeling limitations (Sahmani and Fattahi 2018). More recently some alternative methods have been developed to obtain more accurate results on stability and modal analyzes such quasi-3D refined theory (Sobhy and Zenkour 2019), nonlocal strain gradient theory (Jalaei *et al*. 2019, Sahmani and Safaei 2019, Jalaei and Thai 2019). Also, thermo-mechanical analyzes have gained popularity as the usage of nanomaterials in extreme thermal environments increased dramatically in last decades (Ebrahimi *et al*. 2015, Ebrahimi and Salari 2015, 2016, Ebrahimi and Hosseini 2016, Ebrahimi and Jafari 2016, Ebrahimi and Barati 2016, Ebrahimi and Farazmandnia 2017). In this paper, post-buckling analysis of aorta artery is investigated under axial compression loads on the basis of Euler-Bernoulli beam theory using finite element method.

2. Mechanical model of aorta artery

The main arterial aortic artery, where the whole blood is pumped from the heart to the body, is the aortic artery. As it can be seen from Fig. 1, if we examine the aortic artery from the start (heart) to the end (abdominal arteries); the part of the artery where is attached to the heart is ascending aorta after ascending aorta, the arc with curved structure supplying the brain vasculature and arms is aortic arch, the small part bonding the arc to descending aorta is the thoracic aorta, the most flat and longer part which will be examined in this research coming after thoracic aorta is descending aorta which the buckling case most occurs. In adults, the descending aorta length varies from approximately 4 to 9 cm and is 2-5 mm in diameter (De Garris *et al*. 1933, Presley 1979). Differences in lengths and diameters depend on the height and age. Many studies in the literature have shown that the aortic artery ruptures occur in the descending aortic section (Williams *et al*. 1994), which is the straight vessel in the vein, as shown in Fig. 1. In mechanic modeling, boundary conditions that are the closest to the reality are simple-simple and clamped-clamped support conditions. The aortic artery link in the heart prevents the vein from moving when it does not show rotational resistance, so the support of the aortic artery at the heart side can be compared to the simple support in the mechanical model. Similarly, the other end of the critical part of the aortic artery is connected to the arteries. These artery connections do not show resistance to rotation as they prevent displacement in the same way as they were in the first case, so the other end of the aortic artery can also be called simple support behavior. On the contrary, in some studies in the literature, one end of the artery was assumed to be free and the buckling of the vessel under high pressures was prevented and its behavior under these pressures was examined (Fung *et al*. 1979, Humphrey *et al*. 1993, Kim and Baek 2011, Lillie *et al*. 2010, 2012, Schulze-Bauer *et al*. 2003). Furthermore, after buckling, aorta may behave like fixed from both ends. For this reason, in this research both simple-simple and clamped-clamped boundary condition cases are examined.

The real demonstration of aorta artery together with heart is demonstrated at the left side of the Fig. 1. At the middle, the descending aorta and at the right side of Fig. 1, the continuum model which is used for analyzes is demonstrated.

First three mode shapes and the stable case of descending aorta is demonstrated in Fig. 2. As it can be clearly seen from the figure, with the increase in mode number the length of the descending aorta becomes shorter due to sinusoidal shape.

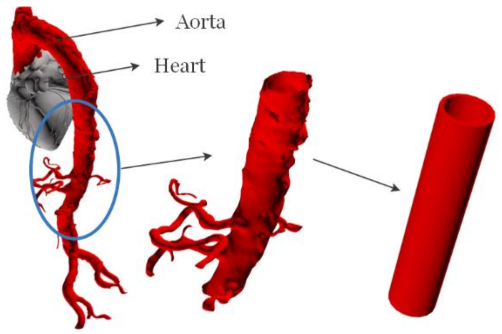

Fig. 1 Transition from real aorta artery to its continuum model

3. Theory and formulations

In the present study, two types of support conditions for the aorta artery are considered. Simply supported-simply supported and simply supported-clamped supported (C-S). Based on Euler-Bernoulli beam theory and Von Karman nonlinear relations, the nonlinear strain-displacement relation is expressed as

$$\varepsilon_{xx} = \frac{du_0}{dx} - z\frac{d^2v_0}{dx^2} + \frac{1}{2}\left(\frac{dv_0}{dx}\right)^2 \tag{1}$$

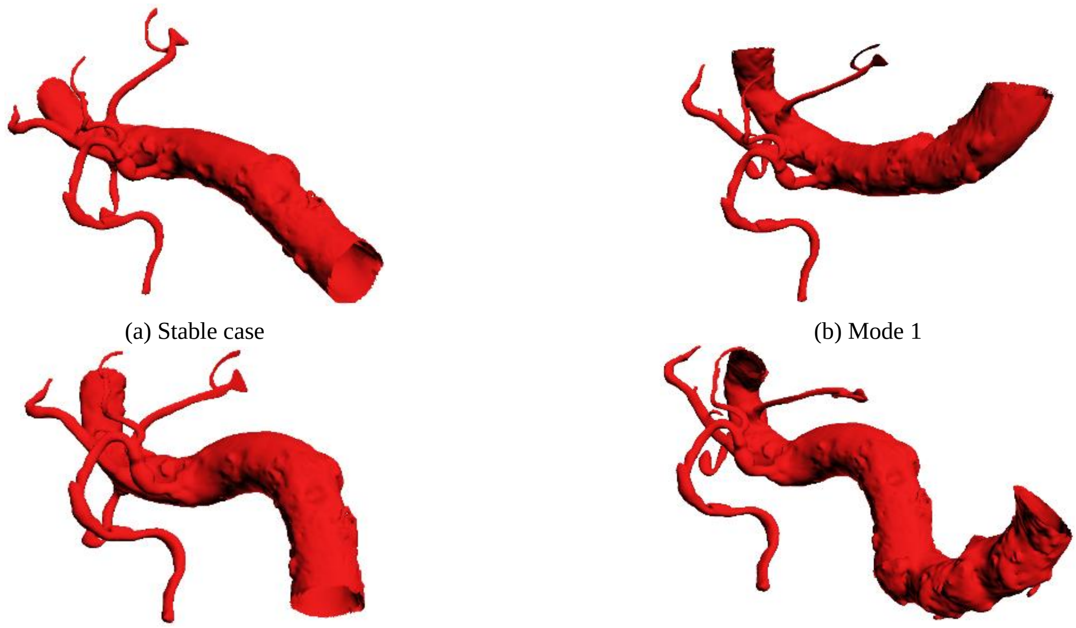

(a) Stable case (b) Mode 1

(c) Mode 2 (d) Mode 3

Fig. 2 First three mode shapes of aorta with its stable case where u_0 and v_0 are the axial and transverse displacements of the midplane, respectively. The constitutive relation of the problem is as follows

$$\sigma_{xx} = E\varepsilon_{xx} \tag{2}$$

Where E is Young Modulus. The stress resultants Nx and Mx represent the axial force and bending moment are given as follow

$$N_x = EA\left[\frac{du_0}{dx} + \frac{1}{2}\left(\frac{dv_0}{dx}\right)^2\right] \tag{3a}$$

$$M_x = -EI\frac{d^2v_0}{dx^2} \tag{3b}$$

The weak form of the problem is as follows (Schembri *et al*. 2004)

$$\begin{aligned}&\int_{x_a}^{x_b}\frac{d\delta u_0}{dx}EA\left[\frac{du_0}{dx} + \frac{1}{2}\left(\frac{dv_0}{dx}\right)^2\right]dx\\ &= \int_{x_a}^{x_b}\delta u_0 f\,dx + \delta u_0(x_a)Q_1 + \delta u_0(x_b)Q_4\end{aligned} \tag{4a}$$

$$\begin{aligned}&\int_{x_a}^{x_b}\left\{\frac{d\delta u_0}{dx}EA\frac{dv_0}{dx}\left[\frac{du_0}{dx} + \frac{1}{2}\left(\frac{dv_0}{dx}\right)^2\right]\right.\\ &\qquad\left. +EI\frac{d^2\delta u_0}{dx^2}\frac{d^2v_0}{dx^2}\right\}dx\\ &= \int_{x_a}^{x_b}\delta v_0 q\,dx + \delta v_0(x_a)Q_2 + \delta v_0(x_b)Q_5\\ &\qquad +\delta\theta(x_a)Q_3 + \delta\theta(x_b)Q_6\end{aligned} \tag{4b}$$

Where f is the external axial force, q is distributed transverse load

$$\begin{aligned}&Q_1 = -N_x(x_a), \qquad Q_4 = N_x(x_b),\\ &Q_2 = -\left[\frac{d\,M_x}{dx} + N_x\frac{dv_0}{dx}\right]_{x_a},\\ &Q_5 = -\left[\frac{d\,M_x}{dx} + N_x\frac{dv_0}{dx}\right]_{x_b},\\ &Q_3 = -M_x(x_a), \qquad Q_4 = M_x(x_b), \qquad \theta = \frac{dv_0}{dx}\end{aligned} \tag{5}$$

For the finite element model of the problem, the nodal displacements q for a two-node beam element contain three degrees of freedom at each node are as follows

$$\begin{aligned}&\{q(t)\}_e\\ &= \left[u_i^{(e)}(t), v_i^{(e)}(t),\ \theta_i^{(e)}(t), u_j^{(e)}(t), v_j^{(e)}(t),\ \theta_j^{(e)}(t)\right]^T\end{aligned} \tag{6}$$

The displacement field of the finite element is expressed in terms of the nodal displacements as follows

$$\begin{aligned}u_0^{(e)}(X,\mathrm{t}) &= \varphi_1^{(U)}(X)\,u_\mathrm{i}(t) + \varphi_2^{(U)}(X)\,u_\mathrm{j}(t)\\ &= \left[\varphi^{(U)}\right]\begin{Bmatrix}u_\mathrm{i}\\ u_\mathrm{j}\end{Bmatrix} = \left[\varphi^{(U)}\right]\{\mathrm{q}\}_U\end{aligned} \tag{7}$$

$$\begin{aligned}v_0^{(\mathrm{e})}(X,\mathrm{t}) &= \varphi_1^{(V)}(X)\,v_\mathrm{i}(t) + \varphi_2^{(V)}(X)\,\theta_\mathrm{i}(t)\\ &+\varphi_3^{(V)}(X)\,v_\mathrm{j}(t) + \varphi_4^{(V)}(X)\,\theta_\mathrm{j}(t)\end{aligned} \tag{8a}$$

$$\left[\varphi^{(V)}\right]\begin{Bmatrix}v_\mathrm{i}\\ \theta_\mathrm{i}\\ v_\mathrm{j}\\ \theta_\mathrm{j}\end{Bmatrix} = \left[\varphi^{(V)}\right]\{q\}_V \tag{8b}$$

where u_i, v_i and θ_i are the axial displacements, transverse displacements and slopes at the two end nodes of the beam element, respectively, and $\varphi_\mathrm{i}^{(U)}$ and $\varphi_\mathrm{i}^{(V)}$ are the Hermitian shape functions for the axial and transverse displacements, respectively. The interpolation functions for the axial displacement are

$$\varphi^{(U)}(\mathrm{X}) = \left[\varphi_1^{(U)}(\mathrm{X})\ \ \varphi_2^{(U)}(\mathrm{X})\right]^T \tag{9}$$

where

$$\varphi_1^{(U)}(\mathrm{X}) = \left(-\frac{X}{L_\mathrm{e}} + 1\right) \tag{10a}$$

$$\varphi_2^{(U)}(\mathrm{X}) = \left(\frac{X}{L_\mathrm{e}}\right) \tag{10b}$$

The interpolation functions for the transverse displacement are

$$\varphi^{(V)}(\mathrm{X}) = \left[\varphi_1^{(V)}(\mathrm{X})\ \ \varphi_2^{(V)}(\mathrm{X})\ \ \varphi_3^{(V)}(\mathrm{X})\ \ \varphi_4^{(V)}(\mathrm{X})\right]^T \tag{11}$$

where

$$\varphi_1^{(V)}(\mathrm{X}) = \left(1 - \frac{3X^2}{L_\mathrm{e}^2} + \frac{2X^3}{L_\mathrm{e}^3}\right) \tag{12a}$$

$$\varphi_2^{(V)}(\mathrm{X}) = \left(-X + \frac{2X^2}{L_\mathrm{e}} - \frac{X^3}{L_\mathrm{e}^3}\right) \tag{12b}$$

$$\varphi_3^{(V)}(\mathrm{X}) = \left(\frac{3X^2}{L_\mathrm{e}^2} - \frac{2X^3}{L_\mathrm{e}^3}\right) \tag{12c}$$

$$\varphi_4^{(V)}(\mathrm{X}) = \left(\frac{X^2}{L_\mathrm{e}} - \frac{2X^3}{L_\mathrm{e}^3}\right) \tag{12d}$$

with L_e indicating the length of the beam element.

Substituting Eqs. (7) and (8) into weak formulation of the problem, and using the usual assemblage procedure of the finite element method, the equations of problem can be obtained for the entire structure as follows

$$[K]\{q(t)\} = \{F\} \tag{13}$$

where [K] is the stiffness matrix and $\{F\}$ is the load vector of the structure. The stiffness matrix [K] can be given as

$$[K] = \begin{bmatrix}[K^A] & [K^B]\\ [K^B]^\mathrm{T} & [K^D]\end{bmatrix} \tag{14}$$

where

$$K^A = \int_{x_a}^{x_b} EA \left[\frac{\partial\varphi^{(U)}}{\partial X}\right]^T \left[\frac{\partial\varphi^{(U)}}{\partial X}\right] dx \tag{15a}$$

$$K^B = \int_{x_a}^{x_b} \frac{1}{2}\left(EA\frac{dv_0}{dx}\right) \left[\frac{\partial\varphi^{(V)}}{\partial X}\right]^T \left[\frac{\partial\varphi^{(U)}}{\partial X}\right] dx \tag{15b}$$

$$K^D = \int_{x_a}^{x_b} \left\{\frac{1}{2}EA\left[\frac{du_0}{dx} + \left(\frac{dv_0}{dx}\right)^2\right] \left[\frac{\partial\varphi^{(V)}}{\partial X}\right]^T \left[\frac{\partial\varphi^{(V)}}{\partial X}\right] + EI\left[\frac{\partial^2\varphi^{(V)}}{\partial X^2}\right]^T \left[\frac{\partial^2\varphi^{(V)}}{\partial X^2}\right]\right\} dx \tag{15c}$$

The load vector $\{F\}$ can be given as

$$\{F\} = \begin{Bmatrix} F_i^1 \\ F_i^2 \end{Bmatrix} \tag{16}$$

where

$$F_i^1 = \int_{x_a}^{x_b} f\left[\varphi^{(U)}\right]^T dx + \varphi_{x_a}^{(U)} Q_1 + \varphi_{x_b}^{(U)} Q_1 \tag{17a}$$

$$F_i^2 = \int_{x_a}^{x_b} q\left[\varphi^{(V)}\right]^T dx + \varphi_{x_a}^{(V)} Q_2 + \varphi_{x_b}^{(V)} Q_5 + \frac{\partial\varphi_{x_a}^{(V)}}{\partial X} Q_3 + \frac{\partial\varphi_{x_b}^{(V)}}{\partial X} Q_6 \tag{17b}$$

For the solution of the nonlinear problem, small-step incremental approaches are used with Newton-Raphson iteration method. For iterations, buckling load is divided using a suitable number according to the value of load. Large numbers are used to divide to loading. Within an iteration process is done, load increment is added to the accumulated load to increase the load. In the Newton-Raphson iteration method, the solution for n+1 th load increment and i th iteration is obtained in the following form

$$R_{n+1}^i = \left(K_T^i\right) du_n^i \tag{18}$$

where K_T^i is the tangent stiffness matrix, du_n^i is the solution increment vector at the i th iteration and n+1 th load increment, $(R_{n+1}^t)_S$ is the system residual vector at the i th iteration and n+1 th load increment. The iteration procedure is continued until the difference between two successive solution vectors is less than a selected tolerance criterion

$$\left|\frac{du_n^{i+1} - du_n^i}{du_n^{i+1}}\right| \le \delta_{tol} \tag{19}$$

In the iteration process, the solution vector is as follows

$$u_{n+1}^{i+1} = u_{n+1}^i + du_{n+1}^i \tag{20}$$

The external load F is divided into several smaller load increments ΔFi

$$F = \sum_{i=1}^{n} \Delta F_i \tag{21}$$

The residual vector for a finite element can be written as

$$\{R\} = [K]\{q(t)\} - \{F\} \tag{22}$$

After the process of the Newton Raphson iteration method, the tangent stiffness matrix is as follows

$$[K_T] = \begin{bmatrix} [K_T^A] & [K_T^B] \\ [K_T^B]^{\mathrm{T}} & [K_T^D] \end{bmatrix} \tag{23}$$

where

$$K_T^A = \int_{x_a}^{x_b} EA \left[\frac{\partial\varphi^{(U)}}{\partial X}\right]^T \left[\frac{\partial\varphi^{(U)}}{\partial X}\right] dx \tag{24a}$$

$$K_T^B = \int_{x_a}^{x_b} \left(EA\frac{dv_0}{dx}\right) \left[\frac{\partial\varphi^{(V)}}{\partial X}\right]^T \left[\frac{\partial\varphi^{(U)}}{\partial X}\right] dx \tag{24b}$$

$$K_T^D = K^D + \int_{x_a}^{x_b} \left\{\frac{1}{2}EA\left[\frac{du_0}{dx} + 2\left(\frac{dv_0}{dx}\right)^2\right] \left[\frac{\partial\varphi^{(V)}}{\partial X}\right]^T \left[\frac{\partial\varphi^{(V)}}{\partial X}\right]\right\} dx \tag{24c}$$

4. Numerical results

In the numerical examples, the post-buckling deflections and critical buckling loads, end calculated and presented in figures for different compressive loads (P) and the geometry parameters of aorta artery. To this end, by use of usual assembly process, the system tangent stiffness matrix and the system residual vector are obtained by using the element stiffness matrixes and element residual vectors for the Euler-Bernoulli beam element and Von-Karman nonlinear relations. After that, the solution process outlined in the previous section is used for obtaining the related solutions for the finite element model of aorta artery element. Three different average diameter is taken into account (D_{avg} = 4.38 mm, D_{avg} = 5.5 mm and D_{avg} = 6 mm). The Young modulus is E = 200 kPa (Han 2007), the thickness is t = 1 mm (except Table 2), the moment of inertia is I = $\pi t R_{avg}^3$

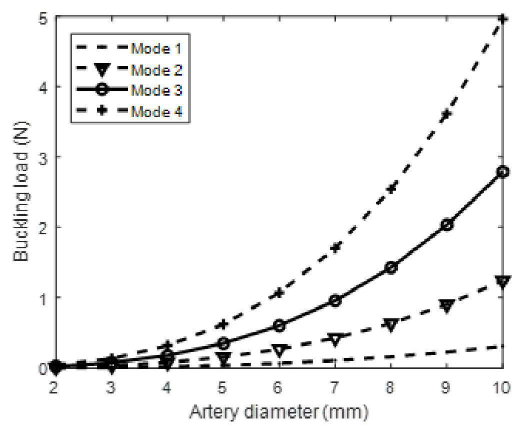

Fig. 3 The buckling load of aorta artery for variable artery diameters for first four modes

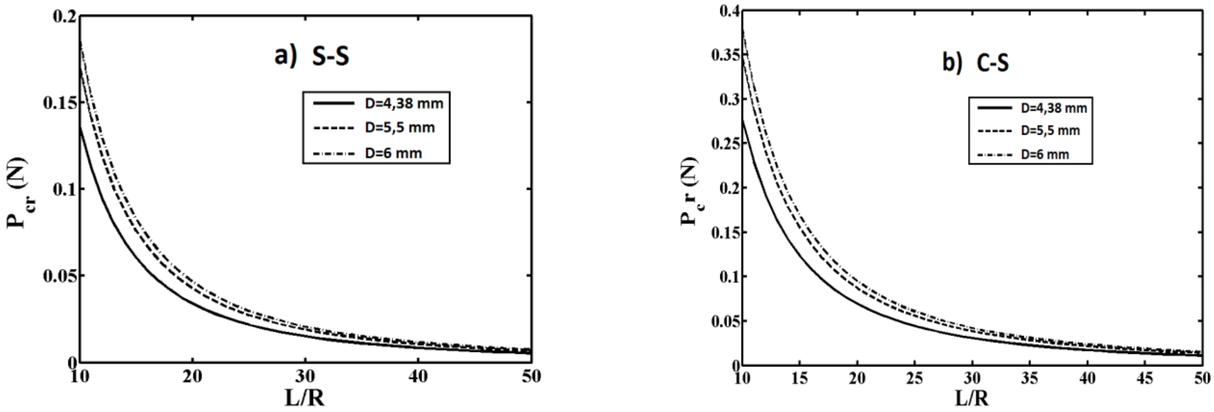

(a) Simply supported (b) Clamped-Simple

Fig. 4 The buckling load of aorta artery for different average diameters and L/R ratios

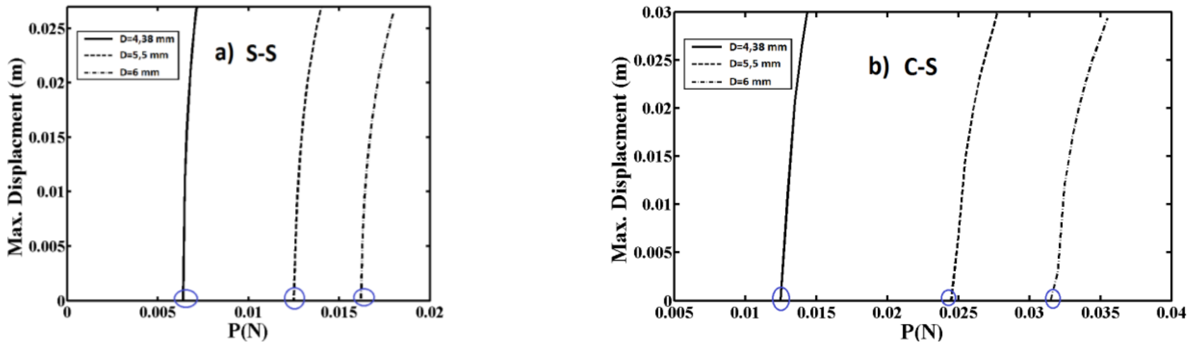

(a) Simply supported (b) Clamped-Simple

Fig. 5 Load- maximum displacements curves of the aorta artery for different average diameters

($R_{avg} = D_{avg}/2$). In the numerical calculations, the number of finite elements is taken as n = 150.

The buckling load of aorta artery for first 4 modes is plotted with variable artery diameters in Fig. 3. In Fig. 4, the effect of the L/R (Length/Radius) on the critical buckling load is presented for different average diameters in both support conditions SS and CS.

The buckling behavior of descending aorta with 50 mm length and 4.38 mm diameter is investigated and results for simply supports are plotted in Fig. 4 and Table 1. As expected, the buckling load is lower for lower mode numbers. Furthermore, increase in diameter also end up with increase in buckling loads while the difference is much bigger for upper mode numbers.

In Table 1, comparative buckling analysis results are given. Classical Euler-Bernoulli buckling theory and finite element software results are compared for first five modes. It is observed that finite element software gives closer results for second and third mode while the difference between results get higher for higher modes.

In Table 2, the effect of arterial wall thickness on its stability is investigated for first ten modes. As expected, thicker arterial wall ends up with stiffer model and higher buckling loads. The software became insufficient to calculate high modes with thinner arterial walls. As it can be clearly seen from Table 2, a slightly difference in arterial wall affect buckling analyses results dramatically.

Table 1 Comparative buckling analysis results of first five modes of aorta for different L/r ratios (N) (Euler-Bernoulli model vs. ANSYS finite element software)

L/r		Mode 1	Mode 2	Mode 3	Mode 4	Mode 5
10	Euler-Bernoulli	0.02605	0.10422	0.23448	0.41686	0.65135
	ANSYS	0.02764	0.11274	0.23962	0.42995	0.66652
20	Euler-Bernoulli	0.01214	0.04212	0.10724	0.17861	0.26456
	ANSYS	0.01342	0.04525	0.11541	0.19141	0.27761
50	Euler-Bernoulli	0.00546	0.01752	0.04272	0.07211	0.11591
	ANSYS	0.00590	0.01862	0.04358	0.07688	0.11726

It is seen from Fig. 4 that the critical buckling load is decreasing significantly with the increasing of the L/R ratio. With increase in the average diameter, the critical buckling load increases inherently. Also, the difference among of diameter values decreases and converge with increase in L/R ratio. After certain L/R in which the results of the different diameters are close and converge to a certain value.

In Fig. 5, the effect of the average diameters on the post-buckling behavior is presented in both support conditions SS and CS. In Fig. 5, the maximum vertical displacements of aorta artery versus compression load rising are presented

Table 2 Buckling analysis results (Newton) of aorta for variable arterial wall thickness (L/r = 10)

Mode	Thickness of arterial wall (t) mm							
	0.5	0.7	0.9	1	1.1	1.3	1.5	2
1	0.022317	0.030195	0.037429	0.041074	0.04407	0.05027	0.056228	0.070585
2	0.058654	0.080217	0.10114	0.11274	0.12209	0.14372	0.16662	0.23135
3	0.099754	0.13868	0.1782	0.20152	0.21962	0.26391	0.31176	0.44952
4	0.1379	0.19587	0.25595	0.2925	0.32019	0.38973	0.46538	0.68431
5	0.16583	0.24542	0.32539	0.37423	0.41165	0.5057	0.60856	0.90715
6	0.17362	0.28089	0.38088	0.43967	0.48728	0.60373	0.7316	1.1031
7	-	0.30218	0,42061	0.4879	0.54568	0.68225	0.8325	1.2678
8	-	0.32696	0.45298	0.52816	0.59189	0.74535	0.91487	1.4034
9	-	-	0.4821	0.56404	0.63111	0.79837	1.0441	1.4447
10	-	-	0.5045	0.59173	0.66312	0.84285	1.0953	1.5201

for the average diameters for the length of aorta artery L = 0.1 m.

As seen from Fig. 5 that increase in the diameter value the displacements, angles and stresses decrease, as expected. With the increase in the compression load, the effects of the diameter on the aorta artery increase significantly. Fig. 5 shows that; the buckling case occurs at the furcation points (see circle) which are bifurcation points. It is known that buckling case occur in either positive or negative directions when the initial arbitrary deviation is affected in the initial position of the aorta artery. The deviation of the direction is taken as positive in this study. Also, these furcation points give the value of the critical buckling load in the figure. It is seen from Fig. 4 that the buckling case occur in bigger loads with increase in the average diameter. It is observed from the results that the diameter value very effective for post-buckling behavior of the aorta artery. Fig. 6 displays the effect of the L/R ratios on the post-buckling displacements of the aorta artery presented in both support conditions SS and CS. In Fig. 5, the maximum vertical displacements of aorta artery versus compression load rising are presented for the L/R ratios for the average diameter D = 6 mm.

It is seen from Fig. 6 that increase in the L/R ratio, the displacements of the aorta artery increase significantly. Also, increase in the L/R ratio, the value of the furcation point (in other word: critical buckling load) decreases seriously. This is because that the aorta artery gets more flexible and slender with increase in the L/R. Another result of the Fig. 5 that the displacement curve close to vertical direction with decrease in the L/R. The displacements reach infinite values in the smaller value of L/R. It is shows that the L/R ratio play important role in the buckling or post-buckling responses of aorta artery.

5. Conclusions

In some biomedical applications, aorta artery under the buckling or post buckling effect. So, during placement of stent some mechanical values must be known. Post-buckling analysis of the aorta artery is studied with different support conditions based on Euler-Bernoulli beam theory and Von Karman nonlinear kinematic relationship by using finite element method. Newton-Raphson iteration method is implemented in the solution of the considered nonlinear problem. The effects of the geometry parameters of the aorta artery on the post-buckling case are investigated and discussed. From these results presented and discussed, the main conclusions are as follows:

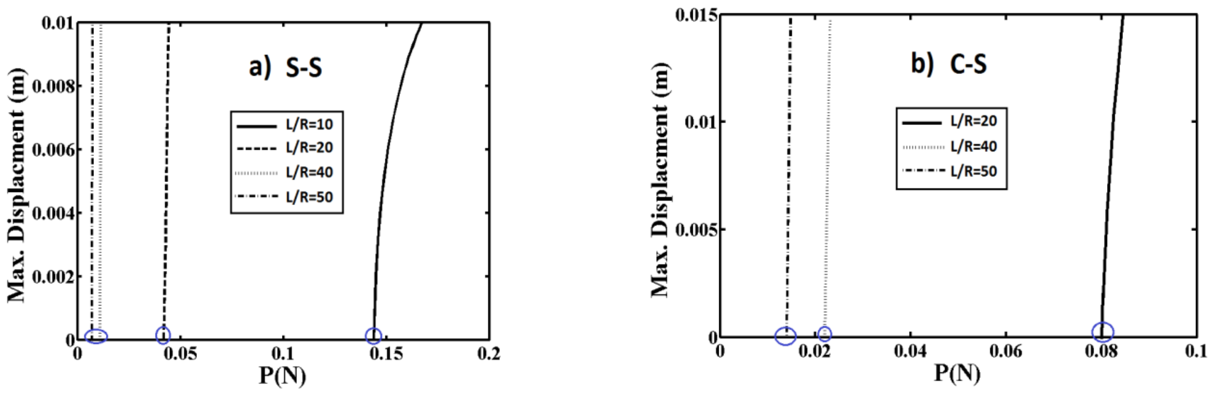

(a) Simply supported (b) Clamped-Simple

Fig. 6 Load- maximum displacements curves of the aorta artery for different L/R ratios

- The diameter value and the L/R ratio are very effective for post-buckling behavior of the aorta artery.
- The difference among of diameter values decreases and converge with increase in L/R ratio.
- With the increase in the compression load, the effects of the diameter on the aorta artery increase.
- The buckling case occur in bigger loads with increase in the average diameter.
- Increase in the L/R ratio, the value of the furcation point decreases seriously.
- The displacements reach infinite values in the smaller value of L/R.
- Future work should be devoted to the interpretation of the results in order to possible the effect of the blood pressure on the post-buckling case. Detailed biomechanical/biomedical studies have cocnluded that mechanical stress concentrations in some effects (for example plaques) play an important parameter in the rupture of plaques. It is possiple to make some study about the determination of stress for buckling behaviour in the plaque, under lumen pressure and axial stretch or other effects. These effects can also be analyzed in the future.

References

Agah, M.R. (2015), "Material characterization of aortic tissue for traumatic injury and buckling", Ph.D. Dissertation; Temple University, PA, USA.

Akgöz, B. and Civalek, O. (2013), "Buckling analysis of functionally graded microbeams based on the strain gradient theory", *Acta Mech.*, **224**(9), 2185-2201. https://doi.org/10.1007/s00707-013-0883-5

Akgöz, B. and Civalek, O. (2014), "Longitudinal vibration analysis for microbars based on strain gradient elasticity theory", *J. Vib. Control*, **20**(4), 606-616. https://doi.org/10.1177%2F1077546312463752

Akgöz, B. and Civalek, O. (2016), "Bending analysis of embedded carbon nanotubes resting on an elastic foundation using strain gradient theory", *Acta Astronaut.*, **119**, 1-12. https://doi.org/10.1016/j.actaastro.2015.10.021

Akgöz, B. and Civalek, O. (2017a), "Effects of thermal and shear deformation on vibration response of functionally graded thick composite microbeams", *Compos. Part B: Eng.*, **129**, 77-87. https://doi.org/10.1016/j.compositesb.2017.07.024

Akgöz, B. and Civalek, O. (2017b), "A size-dependent beam model for stability of axially loaded carbon nanotubes surrounded by Pasternak elastic foundation", *Compos. Struct.*, **176**, 1028-1038. https://doi.org/10.1016/j.compstruct.2017.06.039

Akgöz, B. and Civalek, O. (2017c), "Effects of thermal and shear deformation on vibration response of functionally graded thick composite microbeams", *Compos. Part B: Eng.*, **129**, 77-87. https://doi.org/10.1016/j.compositesb.2017.07.024

ANSYS® Academic Research Mechanical.

Bendaho, B., Belabed, Z., Bourada, M., Benatta, M.A., Bourada, F. and Tounsi, A. (2019), "Assessment of new 2D and quasi-3D nonlocal theories for free vibration analysis of size-dependent functionally graded (FG) nanoplates", *Adv. Nano Res., Int. J.*, **7**(4), 277-292. https://doi.org/10.12989/anr.2019.7.4.277

Berghouti, H., Bedia, E.A.A., Benkhedda, A. and Tounsi, A. (2019), "Vibration analysis of nonlocal porous nanobeams made of functionally graded material", *Adv. Nano Res., Int. J.*, **7**(5), 351-364. https://doi.org/10.12989/anr.2019.7.5.351

Bertrand, S., Cuny, S., Petit, P., Trosseille, X., Page, Y., Guillemot, H. and Drazetic, P. (2008), "Traumatic rupture of thoracic aorta in real-world motor vehicle crashes", *Traffic Inj. Prev.*, **9**(2), 153-161. https://doi.org/10.1080/15389580701775777

Bouadi, A., Bousahla, A.A., Houari, M.S.A., Heireche, H. and Tounsi, A. (2018), "A new nonlocal HSDT for analysis of stability of single layer graphene sheet", *Adv. Nano Res., Int. J.*, **6**(2), 147-162. DOI: https://doi.org/10.12989/anr.2018.6.2.147

Boutaleb, S., Benrahou, K.H., Bakora, A., Algarni, A., Bousahla, A.A., Tounsi, A. and Mahmoud, S.R. (2019), "Dynamic analysis of nanosize FG rectangular plates based on simple nonlocal quasi 3D HSDT", *Adv. Nano Res., Int. J.*, **7**(3), 189-206. https://doi.org/10.12989/anr.2019.7.3.191

Civalek, O. and Demir, C. (2011a), "Buckling and bending analyses of cantilever carbon nanotubes using the euler-bernoulli beam theory based on non-local continuum model", *Asian J. Civil Eng.*, **12**(5), 651-661.

Civalek, O. and Demir, C. (2011b), "Bending analysis of microtubules using nonlocal Euler-Bernoulli beam theory", *Appl. Math. Model.*, **35**(5), 2053-2067. https://doi.org/10.1016/j.apm.2010.11.004

Civalek, O. and Demir, C. (2016), "A simple mathematical model of microtubules surrounded by an elastic matrix by nonlocal finite element method", *Appl. Math. Comput.*, **289**, 335-352. https://doi.org/10.1016/j.amc.2016.05.034

Civalek, O. and Kiracioglu, O. (2010), "Free vibration analysis of Timoshenko beams by DSC method", *Int. J. Num. Method. Biomed. Eng.*, **26**(12), 1890-1898. https://doi.org/10.1002/cnm.1279

De Garis, C.F., Black, I.H. and Riemenschneider, E.A. (1933), "Patterns of the Aortic Arch in American White and Negro Stocks, with Comparative Notes on Certain Other Mammals", *J. Anat.*, **67**, 599-619.

Demir, C. and Civalek, O. (2013), "Torsional and longitudinal frequency and wave response of microtubules based on the nonlocal continuum and nonlocal discrete models", *Appl. Math. Model.*, **37**(22), 9355-9367. https://doi.org/10.1016/j.apm.2013.04.050

Demir, Ç. and Civalek, O. (2017a), "On the analysis of microbeams", *Int. J. Eng. Sci.*, **121**, 14-33. https://doi.org/10.1016/j.ijengsci.2017.08.016

Demir, Ç. and Civalek, O. (2017b), "A new nonlocal FEM via Hermitian cubic shape functions for thermal vibration of nano beams surrounded by an elastic matrix", *Compos. Struct.*, **168**, 872-884. https://doi.org/10.1016/j.compstruct.2017.02.091

Demir, C., Akgoz, B., Erdinç, M.C., Mercan, K. and Civalek, O. (2017), "Free vibration analysis of graphene sheets on elastic matrix", *J. Fac. Eng. Archit. Gazi Univ.*, **32**(2), 551-562. https://dx.doi.org/10.17341/gummfd.61874

Ebrahimi, F. and Barati, M.R. (2016), "Dynamic modeling of a thermo–piezo-electrically actuated nanosize beam subjected to a magnetic field", *Appl. Phys. A*, **122**(4), 451. https://doi.org/10.1007/s00339-016-0001-3

Ebrahimi, F. and Barati, M.R. (2017), "Small-scale effects on hygro-thermo-mechanical vibration of temperature-dependent nonhomogeneous nanoscale beams", *Mech. Adv. Mater. Struct.*, **24**(11), 924-936. https://doi.org/10.1080/15376494.2016.1196795

Ebrahimi, F. and Barati, M.R. (2018), "Vibration analysis of smart piezoelectrically actuated nanobeams subjected to magneto-electrical field in thermal environment", *J. Vib. Control*, **24**(3), 549-564. https://doi.org/10.1177%2F1077546316646239

Ebrahimi, F. and Farazmandnia, N. (2017), "Thermo-mechanical vibration analysis of sandwich beams with functionally graded carbon nanotube-reinforced composite face sheets based on a higher-order shear deformation beam theory", *Mech. Adv. Mater. Struct.*, **24**(10), 820-829.

https://doi.org/10.1080/15376494.2016.1196786

Ebrahimi, F. and Hosseini, S.H.S. (2016), "Thermal effects on nonlinear vibration behavior of viscoelastic nanosize plates", *J. Therm. Stress*., **39**(5), 606-625. https://doi.org/10.1080/01495739.2016.1160684

Ebrahimi, F. and Jafari, A. (2016), "A higher-order thermomechanical vibration analysis of temperature-dependent FGM beams with porosities", *J. Eng*., 9561504. https://doi.org/10.1155/2016/9561504

Ebrahimi, F. and Salari, E. (2015), "Size-dependent thermo-electrical buckling analysis of functionally graded piezoelectric nanobeams", *Smart Mater. Struct*., **24**(12), 125007. https://doi.org/10.1088/0964-1726/24/12/125007

Ebrahimi, F. and Salari, E. (2016), "Effect of various thermal loadings on buckling and vibrational characteristics of nonlocal temperature-dependent functionally graded nanobeams", *Mech. Adv. Mater. Struct*., **23**(12), 1379-1397. https://doi.org/10.1080/15376494.2015.1091524

Ebrahimi, F., Salari, E. and Hosseini, S.A.H. (2015), "Thermomechanical vibration behavior of FG nanobeams subjected to linear and non-linear temperature distributions", *J. Therm. Stress*., **38**(12), 1360-1386. https://doi.org/10.1080/01495739.2015.1073980

Ebrahimi, F., Babaei, R. and Shaghaghi, G.R. (2018), "Vibration analysis thermally affected viscoelastic nanosensors subjected to linear varying loads", *Adv. Nano Res., Int. J.*, **6**(4), 399-422. https://doi.org/10.12989/anr.2018.6.4.399

Ebrahimi, F., Karimiasl, M. and Mahesh, V. (2019), "Vibration analysis of magneto-flexo-electrically actuated porous rotary nanobeams considering thermal effects via nonlocal strain gradient elasticity theory", *Adv. Nano Res., Int. J.*, **7**(4), 221-231. https://doi.org/10.12989/anr.2019.7.4.221

Fantuzzi, N., Tornabene, F., Bacciocchi, M. and Dimitri, R. (2017), "Free vibration analysis of arbitrarily shaped Functionally Graded Carbon Nanotube-reinforced plates", *Compos. Part B: Eng*., **115**, 384-408. https://doi.org/10.1016/j.compositesb.2016.09.021

Fung, Y.C., Fronek, K. and Patitucci, P. (1979), "Pseudoelasticity of arteries and the choice of its mathematical expression", *Am. J. Physiol. Heart and Circ. Physiol*., **237**(5), H620-H631. https://doi.org/10.1152/ajpheart.1979.237.5.H620

Gammie, J.S., Shah, A.S., Hattler, B.G., Kormos, R.L., Peitzman, A.B., Griffith, B.P. and Pham, S.M. (1998), "Traumatic aortic rupture: diagnosis and management", *Ann. Thorac. Surg.*, **66**(4), 1295-1300. https://doi.org/10.1016/S0003-4975(98)00778-4

Garcia, J.R., Lamm, S.D. and Han, H.C. (2013), "Twist buckling behavior of arteries", *Biomech. Model. Mechanobiol.*, **12**(5), 915-927. https://doi.org/10.1007/s10237-012-0453-0

Garcia, J.R., Sanyal, A., Fatemifar, F., Mottahedi, M. and Han, H.C. (2017), "Twist buckling of veins under torsional loading", *J. Biomech.*, **58**, 123-130. https://doi.org/10.1016/j.jbiomech.2017.04.018

Gore, R.W. (1974), "Pressures in cat mesenteric arterioles and capillaries during changes in systemic arterial blood pressure", *Circ. Res.*, **34**, 581-591. https://doi.org/10.1161/01.RES.34.4.581

Gore, R.W. and Bohlen, H. (1975), "Pressure regulation in the microcirculation", *Fed. Proceed.*, **34**(11), 2031-2037.

Han, H.C. (2007), "A biomechanical model of artery buckling", *J. Biomech*., **40**(16), 3672-3678. https://doi.org/10.1016/j.jbiomech.2007.06.018

Han, H.C. (2009a), "The mechanical buckling of curved arteries", *Mol. Cell. Biomech*., **6**(2), 93-99. http://test.techscience.com/mcb/v6n2/28480

Han, H.C. (2009b), "The theoretical foundation for artery buckling under internal pressure", *J. Biomech. Eng.*, **131**(12), 124501. https://doi.org/10.1115/1.4000080

Han, H.C., Chesnutt, J.K., Garcia, J.R., Liu, Q. and Wen, Q. (2013), "Artery buckling: new phenotypes, models, and applications", *Ann. Biomed. Eng*., **41**(7), 1399-1410. https://doi.org/10.1007/s10439-012-0707-0

Hayman, D.M., Zhang, J., Liu, Q., Xiao, Y. and Han, H.C. (2013), "Smooth muscle cell contraction increases the critical buckling pressure of arteries", *J. Biomech*., **46**(4), 841-844. https://doi.org/10.1016/j.jbiomech.2012.11.040

Humphrey, J., Kang, T., Sakarda, P. and Anjanappa, M. (1993), "Computer-aided vascular experimentation: a new electromechanical test system", *Ann. Biomed. Eng.*, **21**(1), 33-43. https://doi.org/10.1007/BF02368162

Jainandunsing, J.S., Linnemann, R., Bouma, W., Natour, N., Bidar, E., Lorusso, R., Gelsomino, S., Johnson, D.M. and Natour, E. (2019), "Aorto-atrial fistula formation and closure: a systematic review", *J. Thorac. Dis.*, **11**, 1031-1046. https://dx.doi.org/10.21037%2Fjtd.2019.01.7

Jalaei, M.H. and Arani, A.G. (2018), "Size-dependent static and dynamic responses of embedded double-layered graphene sheets under longitudinal magnetic field with arbitrary boundary conditions", *Compos. Part B: Eng*., **142**, 117-130. https://doi.org/10.1016/j.compositesb.2017.12.053

Jalaei, M.H. and Thai, H.T. (2019), "Dynamic stability of viscoelastic porous FG nanoplate under longitudinal magnetic field via a nonlocal strain gradient quasi-3D theory", *Compos. Part B: Eng*., **175**, 107164. https://doi.org/10.1016/j.compositesb.2019.107164

Jalaei, M.H., Arani, A.G. and Tourang, H. (2018), "On the dynamic stability of viscoelastic graphene sheets", *Int. J Eng. Sci*., **132**, 16-29. https://doi.org/10.1016/j.ijengsci.2018.07.002

Jalaei, M.H., Arani, A.G. and Nguyen-Xuan, H. (2019), "Investigation of thermal and magnetic field effects on the dynamic instability of FG Timoshenko nanobeam employing nonlocal strain gradient theory", *Int. J. Mech. Sci.*, **161**, 105043. https://doi.org/10.1016/j.ijmecsci.2019.105043

Jezkova, K., Rathouska, J., Nemeckova, I., Fikrova, P., Dolezelova, E., Varejckova, M., Vitverova, B., Bernabeu, C., Novoa, J.M., Chlopicki, S. and Nachtigal, P. (2016), "Vascular Biology: Endothelium and Smooth Muscle Cells. High Levels of Soluble Endoglin Induce Inflammation and Oxidative Stress in Aorta Compensated with Preserved No-Dependent Vasodilatation Mice Fed High Fat Diet", *Atheroscler*., **252**, E160-E160. https://doi.org/10.1016/j.atherosclerosis.2016.07.771

Kaniowsk, T., Bross, T., Koltowsk, R., Kustrzyc, A. and Olejak, B. (1970), "Kinking or Buckling of Aorta", *Pol. Rev. Radiol. Nucl. Med*., **34**, 187-+.

Kheroubi, B., Benzair, A., Tounsi, A. and Semmah, A. (2016), "A new refined nonlocal beam theory accounting for effect of thickness stretching in nanoscale beams", *Adv. Nano Res., Int. J*., **4**(4), 251-264. https://doi.org/10.12989/anr.2016.4.4.251

Kim, J. and Baek, S. (2011), "Circumferential variations of mechanical behavior of the porcine thoracic aorta during the inflation test", *J. Biomech*., **44**(10), 1941-1947. https://doi.org/10.1016/j.jbiomech.2011.04.022

Lee, W.A., Matsumura, J.S., Mitchell, R.S., Farber, M.A., Greenberg, R.K., Azizzadeh, A., Murad, M.H. and Fairman, R.M. (2011), "Endovascular repair of traumatic thoracic aortic injury: clinical practice guidelines of the Society for Vascular Surgery", *J. Vasc. Surg.*, **53**(1), 187-192. https://doi.org/10.1016/j.jvs.2010.08.027

Levesque, M. and Nerem, R. (1985), "The elongation and orientation of cultured endothelial cells in response to shear stress", *J. Biomech. Eng*., **107**, 341-347. https://doi.org/10.1115/1.3138567

Levy, B.I. and Tedgui, A. (2007), *Biology of the Arterial Wall Vol. 1*, Springer Science & Business Media, MA, Boston, USA.

Lillie, M., Shadwick, R. and Gosline, J. (2010), "Mechanical anisotropy of inflated elastic tissue from the pig aorta", *J.*

Biomech., **43**(11), 2070-2078.
https://doi.org/10.1016/j.jbiomech.2010.04.014

Lillie, M., Armstrong, T., Gérard, S., Shadwick, R. and Gosline, J. (2012), "Contribution of elastin and collagen to the inflation response of the pig thoracic aorta: assessing elastin's role in mechanical homeostasis", *J. Biomech*., **45**(12), 2133-2141.
https://doi.org/10.1016/j.jbiomech.2012.05.034

Liu, Q. and Han, H.C. (2012), "Mechanical buckling of artery under pulsatile pressure", *J. Biomech*., **45**(7), 1192-1198.
https://doi.org/10.1016/j.jbiomech.2012.01.035

Liu, Q., Wen, Q., Mottahedi, M. and Han, H.C. (2014), "Artery buckling analysis using a four-fiber wall model", *J. Biomech.*, **47**(11), 2790-2796. https://doi.org/10.1016/j.jbiomech.2014.06.005

Martinez, R., Fierro, C.A., Shireman, P.K. and Han, H.C. (2010), "Mechanical Buckling of Veins Under Internal Pressure", *Ann. Biomed. Eng*., **38**(4), 1345-1353.
https://doi.org/10.1007/s10439-010-9929-1

Mercan, K. and Civalek, O. (2017), "Buckling analysis of Silicon carbide nanotubes (SiCNTs) with surface effect and nonlocal elasticity using the method of HDQ", *Compos. Part B: Eng*., **114**, 34-45. https://doi.org/10.1016/j.compositesb.2017.01.067

Mulvany, M. and Aalkjaer, C. (1990), "Structure and function of small arteries", *Physiol. Rev*., **70**, 921-961.
https://doi.org/10.1152/physrev.1990.70.4.921

Numanoğlu, H.M., Akgöz, B. and Civalek, O. (2018), "On dynamic analysis of nanorods", *Int. J. Eng. Sci*., **130**, 33-50.
https://doi.org/10.1016/j.ijengsci.2018.05.001

Presley, R. (1979), "The primitive course of the internal carotid artery in mammals", *Cell. Tissue. Organ*., **103**(2), 238-244.
https://doi.org/10.1159/000145015

Rachev, A.A. (2009), "Theoretical study of mechanical stability of arteries", *J. Biomech. Eng*., **131**(5), 051006.
https://doi.org/10.1115/1.3078188

Richens, D., Kotidis, K., Neale, M., Oakley, C. and Fails, A. (2003), "Rupture of the aorta following road traffic accidents in the United Kingdom 1992–1999. The results of the co-operative crash injury study", *Eur. J. Cardiothorac. Surg*., **23**(2), 143-148.
https://doi.org/10.1016/S1010-7940(02)00720-0

Sahmani, S. and Fattahi, A.M.B. (2018), "Development of efficient size-dependent plate models for axial buckling of single-layered graphene nanosheets using molecular dynamics simulation", *Microsyst. Technol*., **24**, 1265-1277.
https://doi.org/10.1007/s00542-017-3497-3

Sahmani, S. and Safaei, B. (2019), "Nonlinear free vibrations of bi-directional functionally graded micro/nano-beams including nonlocal stress and microstructural strain gradient size effects", *Thin-Wall. Struct.*, **140**, 342-356.
https://doi.org/10.1016/j.tws.2019.03.045

Schembri, P., Crane, D.L. and Reddy, J.N. (2004), "A three-dimensional computational procedure for reproducing meshless methods and the finite element method", *Int. J. Numer. Method. Eng*., **61**(6), 896-927. https://doi.org/10.1002/nme.1095

Schulze-Bauer, C.A., Mörth, C. and Holzapfel, G.A. (2003), "Passive biaxial mechanical response of aged human iliac arteries", *J. Biomech. Eng*., **125**(3), 395-406.
https://doi.org/10.1115/1.1574331

Semmah, A., Heireche, H., Bousahla, A.A. and Tounsi, A. (2019), "Thermal buckling analysis of SWBNNT on Winkler foundation by nonlocal FSDT", *Adv. Nano Res., Int. J.*, **7**(2), 89-98.
https://doi.org/10.12989/anr.2019.7.2.089

Smyth, P.T. and Edwards, J.E. (1972), "Pseudocoarctation, kinking or buckling of the aorta", *Circ.*, **46**(5), 1027-1032.
https://doi.org/10.1161/01.CIR.46.5.1027

Sobhy, M. and Zenkour, A.M. (2019), "Porosity and inhomogeneity effects on the buckling and vibration of double-FGM nanoplates via a quasi-3D refined theory", *Compos. Struct*., **220**, 289-303.
https://doi.org/10.1016/j.compstruct.2019.03.096

Tornabene, F., Fantuzzi, N., Bacciocchi, M. and Dimitri, R. (2015a), "Dynamic analysis of thick and thin elliptic shell structures made of laminated composite materials", *Compos. Struct*., **133**, 278-299.
https://doi.org/10.1016/j.compstruct.2015.06.052

Tornabene, F., Fantuzzi, N., Bacciocchi, M. and Viola, E. (2015b), "Higher-order theories for the free vibrations of doubly-curved laminated panels with curvilinear reinforcing fibers by means of a local version of the GDQ method", *Compos. Part B: Eng*., **81**, 196-230. https://doi.org/10.1016/j.compositesb.2015.07.012

Williams, J.S., Graff, J.A., Uku, J.M. and Steinig, J.P. (1994), "Aortic injury in vehicular trauma", *Ann. Thorac. Surg*., **57**(3), 726-730. https://doi.org/10.1016/0003-4975(94)90576-2

Youcef, D.O., Kaci, A., Houari, M.S.A., Tounsi, A., Benzair, A. and Heireche, H. (2015), "On the bending and stability of nanowire using various HSDTs", *Adv. Nano Res., Int. J.*, **3**(4), 177-191. https://doi.org/10.12989/anr.2015.3.4.177

Zhang, J., Liu, Q. and Han, H.C. (2014), "An in vivo rat model of artery buckling for studying wall remodeling", *Ann. Biomed. Eng.*, **42**(8), 1658-1667.
https://doi.org/10.1007/s10439-014-1017-5

CC